





Article

Magnetized Flow of Cu + Al₂O₃ + H₂O Hybrid Nanofluid in Porous Medium: Analysis of Duality and Stability

Liaquat Ali Lund ^{1,2}, Zurni Omar ¹, Sumera Dero ³ , Ilyas Khan ^{4,*} , Dumitru Baleanu ^{5,6,7}  and Kottakkaran Soopy Nisar ⁸ 

- ¹ School of Quantitative Sciences, Universiti Utara Malaysia, Sintok 06010, Malaysia; liaquat_ali@ahsgs.uum.edu.my or balochliaqatali@gmail.com (L.A.L.); zurni@uum.edu.my (Z.O.)
 - ² KCAET Khairpur Mirs, Sindh Agriculture University, Tandojam Sindh 70060, Pakistan
 - ³ Faculty of Engineering and Technology, University of Sindh, Jamshoro 76080, Pakistan; sumera.dero@usindh.edu.pk
 - ⁴ Faculty of Mathematics and Statistics, Ton Duc Thang University, Ho Chi Minh City 72915, Vietnam
 - ⁵ Department of Mathematics, Cankaya University, Ankara 06790, Turkey; dumitru@cankaya.edu.tr or Baleanu@mail.cmuh.org.tw
 - ⁶ Institute of Space Sciences, 077125 Magurele, Romania
 - ⁷ Department of Medical Research, China Medical University Hospital, China Medical University, Taichung 40447, Taiwan
 - ⁸ Department of Mathematics, College of Arts and Sciences, Prince Sattam bin Abdulaziz University, Wadi Aldawaser 11991, Saudi Arabia; n.soopy@psau.edu.sa
- * Correspondence: ilyaskhan@tdtu.edu.vn

Received: 14 August 2020; Accepted: 9 September 2020; Published: 14 September 2020



Abstract: In this analysis, we aim to examine the heat transfer and flow characteristics of a copper-aluminum/water hybrid nanofluid in the presence of viscous dissipation, magnetohydrodynamic (MHD), and porous medium effect over the shrinking sheet. The governing equations of the fluid model have been acquired by employment of the model of Tiwari and Das, with additional properties of the hybrid nanofluid. The system of partial differential equations (PDEs) has been converted into ordinary differential equations (ODEs) by adopting the exponential similarity transformation. Similarity transformation is an essential class of phenomenon where the symmetry of the scale helps to reduce the number of independent variables. Note that ODE solutions demonstrate the PDEs symmetrical behavior for the velocity and temperature profiles. With BVP4C solver in the MATLAB program, the system of resulting equations has been solved. We have compared the present results with the published results and found in excellent agreements. The findings of the analysis are also displayed and discussed in depth graphically and numerically. It is discovered that two solutions occur in definite ranges of suction and magnetic parameters. Dual (no) similarity solutions can be found in the range of $S_c \leq S$ and $M_c \leq M$ ($S_c > S$ and $M_c > M$). By performing stability analysis, the smallest values of eigenvalue are obtained, suggesting that a stable solution is the first one. Furthermore, the graph of the smallest eigenvalue shows symmetrical behavior. By enhancing the Eckert number values the temperature of the fluid is raised.

Keywords: hybrid nanofluid; porous medium; dual solutions; viscous dissipation; stability analysis

1. Introduction

The concept of nanofluid was first proposed in 1995, by Choi and Eastman [1]. In their spearheading research, they found that the enhancement of the heat transfer rate in nanofluid is higher

as compared to any kind of simple viscous fluids. It is made by mixing solid nanoparticles in the base fluids [2]. Until now, various kinds of base fluids with different kinds of solid nanoparticles have been mixed and examined in the literature. Nanoparticles can be polymeric nanoparticles, magnetic nanoparticles, dendrimers, liposomes, metallic nanoparticles, quantum dots, and numerous others. The ethylene glycol, water, oil, sodium alginate and, etc. can be used as the base fluids. Further, carbon nanotubes and the well-known graphite are categorized as the no-metallic nanoparticles, while nitrides, metal oxides, copper, carbides, and, alumina are the metallic nanoparticles. Ghazvini et al. [3] used an experimental approach to examine the water-based nanofluid which contained the CuFe_2O_4 nanoparticles. Tassaddiq et al. [4] investigated the sodium alginate nanofluid through a numerical approach where they used the model of Brinkman. Molybdenum disulphide (MoS_2) nanoparticles were considered as solid particles. Further, single-wall carbon nanotubes (SWCNT) and multi-wall carbon nanotubes (MWCNT) carbon nanotubes in the water base fluid were considered by Nadeem et al. [5]. Mitra et al. [6] tried to find the maximum heat transfer rate of TiO_2 in the examination by considering the various sizes and phases of the nanoparticles. Sahoo and Kumar [7] investigated the various mixtures of nanoparticles in order to find the maximum heat transfer rate. In this regard, three nanoparticles Al_2O_3 , CuO , and TiO_2 were considered, and also $\text{Al}_2\text{O}_3\text{-CuO-TiO}_2$ ternary hybrid nanofluid were examined. Shafiq et al. [8] numerically examined the single-and multi-wall carbon nanotubes. Further, Gireesha et al. [9] used a two-phase nanofluid model to investigate Jeffrey nanofluid in a three-dimensional framework. Lund et al. [10] used the same model of Gireesha et al. [9] for the examination of the micropolar nanofluid. It is worth mentioning here that various mixes of nanoparticles in the different base fluids have been investigated. Nevertheless, nobody concluded which nanoparticle mixture and base fluid may offer superior heat transfer rate improvement (refer to the work of [11–18]).

The new development in the innovation of technologies required more heat transfer rates. The most recent investigation of the nanofluids revealed that the better heat transfer rate can be achieved with a new kind of nanofluid which is a hybrid nanofluid. It is composed by dispersing two different types of nanoparticles in the base fluid. This new kind of nanofluid can support the technologies of the industries and engineering with the minimum cost as it works effectively in vehicle thermal management/engine cooling, generator cooling, heating and cooling in buildings, biomedical, electronic cooling, nuclear system cooling, etc. By suspending the suitable combination of nanoparticles, even for the small volume fraction of nanoparticles, the required effects of heat transfer rate can be achieved [19]. However, not many investigations were accounted for on the synthesis and preparation of the hybrid nanofluid as it is a new kind of fluid [20]. It tends to be closed from the overview of the published literature that the exceptionally limited studies have been focused on the heat transfer and the fluid flow of the hybrid nanofluids numerically. Lund et al. [21] considered the shrinking surface to investigate the hybrid nanofluid by considering copper and alumina as solid particles and found double solutions. We have looked at Devi and Devi's thermophysical model [22]. Devi and Devi [22] compared their numerical findings with the experimental outcomes of Suresh et al. [23] and found a good contrast between them. Therefore, it can be expected that our present results would be beneficial for those who are working in this area, as the model of Devi and Devi [23] has good validation with the experimental work. Hayat and Nadeem [24] investigated the hybrid nanofluid and found that hybrid nanofluid has more capacity to transfer heat than simple nanofluid. Jamshed et al. [25] studied hybrid nanofluid using engine oil as the regular fluid and observed that higher heat transfer is possible only for minimum value of shape feature parameter. Dual solutions with stability analysis of stagnation point flow of hybrid nanofluid were examined by Rostami et al. [26]. The magnetohydrodynamic (MHD) flow from hybrid Nanofluid based on water over shrinking/stretching sheets has been studied by Aly and Pop [27] and double solutions have been found. In comparison with the hybrid nanofluid $\text{TiO}_2\text{-Cu/H}_2\text{O}$, Khan et al. [28] revealed that the lower Nusselt is the Cu-Water nanofluid. Olatundun and Makinde [29] modified the model of Blasius for the hybrid nanofluid in which convective condition had also been considered. Chamkha et al. [30] examined the hybrid nanofluid in the rotating system where they found that "Nusselt number acts as an ascending function of injection and

radiation parameters, as well as volume fraction of nanofluid". Maskeen et al. [31] investigated the hydromagnetic alumina–copper/water hybrid nanofluid. An interesting development of the hybrid nanofluid can be seen in these papers [32–38].

The exponentially shrinking/stretching surface is commonly utilized with the fluid flow and the heat transfer in daily life and industrial problems. It seems that the Magyari and Keller [39] paper is the first paper on the exponentially stretching sheet to look at the fluid boundary layer flow. Mushtaq et al. [40] utilized the exponential similarity variables to transform the governing PDEs into ODEs. Further, Reddy et al. [41] considered the mixed convection flow of nanofluid over the exponential surface where they found that for the highest value of viscous ratio parameter then concentration, momentum, thermal boundary layers thicknesses enhance. Rahman et al. [42] developed the MHD flow model for the stagnation point where exponential similarity variables were used to get ODEs. Some studies of fluid flow over the exponential surface can be found in these articles [43–47]. Bachok et al. [48] used a single-phase model of nanofluid over the exponential surface and concluded that two solutions existed in an exponentially shrinking sheet. Moreover, unsteady stagnation point flow of nanofluid was considered by Dzulkipli et al. [49]. Anuar et al. [50] examined the hybrid nanofluid flow over an exponential sheet and noticed double solutions. Meanwhile, the stability of the solutions was also evaluated because solutions were not uniquely present. Waini et al. [51] have recently considered and obtained two branches for a hybrid nanofluid MHD flow in the impact of the heat radiation effect. They considered alumina and copper as the nanoparticles with water and concluded that heat transfer was reduced in both solutions when the thermal radiation parameter was enhanced.

In this study, we have extended the research of the Waini et al. [51] to examine the MHD flow of the $\text{Al}_2\text{O}_3\text{-Cu/water}$ hybrid on the exponentially shrinking sheet. Moreover, the effects of the porous medium and viscous dissipation have been taken into account. By applying exponential similarity transformation variables, momentum, and energy conservations are converted to the system of ODEs. The numerical solutions of the resulting equations have been determined by employing the shooting technique. Further, analysis of the stability of solutions has also been performed to specify a stable solution with a bvp4c solver. The effects of the different application parameters are shown graphically on the heat transfer rate and skin friction coefficient. Lastly, this work can be extended in the following directions: (i) considering the vertical exponential surface with thermal radiation effect; (ii) considering the first and second-order slip conditions, and (iii) considering the entire model for the three-dimensional flow.

2. Mathematical Modeling

Let us take the two-dimensional, steady, MHD, and incompressible flow of a hybrid nanofluid in the presence of viscous dissipation and porosity on the exponentially shrinking surface (allude to Figure 1). The governing momentum, mass, and energy conservation are expressed in the following terms by considering all assumptions (see [51–53]):

$$\frac{\partial u}{\partial x} + \frac{\partial v}{\partial y} = 0 \quad (1)$$

$$u \frac{\partial u}{\partial x} + v \frac{\partial u}{\partial y} = \frac{\mu_{hnf}}{\rho_{hnf}} \frac{\partial^2 u}{\partial y^2} - \frac{\mu_{hnf}}{\rho_{hnf} K} u - \frac{\sigma_{hnf}}{\rho_{hnf}} B^2 u \quad (2)$$

$$u \frac{\partial T}{\partial x} + v \frac{\partial T}{\partial y} = \frac{k_{hnf}}{(\rho c_p)_{hnf}} \frac{\partial^2 T}{\partial y^2} + \frac{\mu_{hnf}}{(\rho c_p)_{hnf}} \left(\frac{\partial u}{\partial y} \right)^2 \quad (3)$$

The boundary conditions are

$$\begin{cases} v = v_w(x), u = u_w, T = T_w \text{ as } y = 0 \\ u \rightarrow 0, T \rightarrow T_\infty, \text{ as } y \rightarrow \infty \end{cases} \quad (4)$$

here, velocities along the y -axis and x -axis are v and u , respectively, T and $T_w(x)$ are the temperature of fluid and surface, respectively, where $T_w(x) = T_\infty + T_0 e^{\frac{x}{2l}}$, T_∞ is free stream temperature, $B = B_0 e^{\frac{x}{2l}}$ is the field of magnetic where B_0 is constant magnetic strength, $K = 2K_0 e^{\frac{x}{2l}}$ is considered as the permeability of porous medium where K_0 is the reference permeability, $(\rho c_p)_{hnf}$, ρ_{hnf} , σ_{hnf} , k_{hnf} , and μ_{hnf} , are corresponding effective heat capacity, density, electrical conductivity, thermal conductivity, and viscosity of hybrid nanofluid. Further, $u_w = -U_w e^{\frac{x}{2l}}$ is the surface velocity, and $v_w = \sqrt{\frac{\delta_f U_w}{2l}} e^{\frac{x}{2l}} S$ where S is blowing/suction parameter.

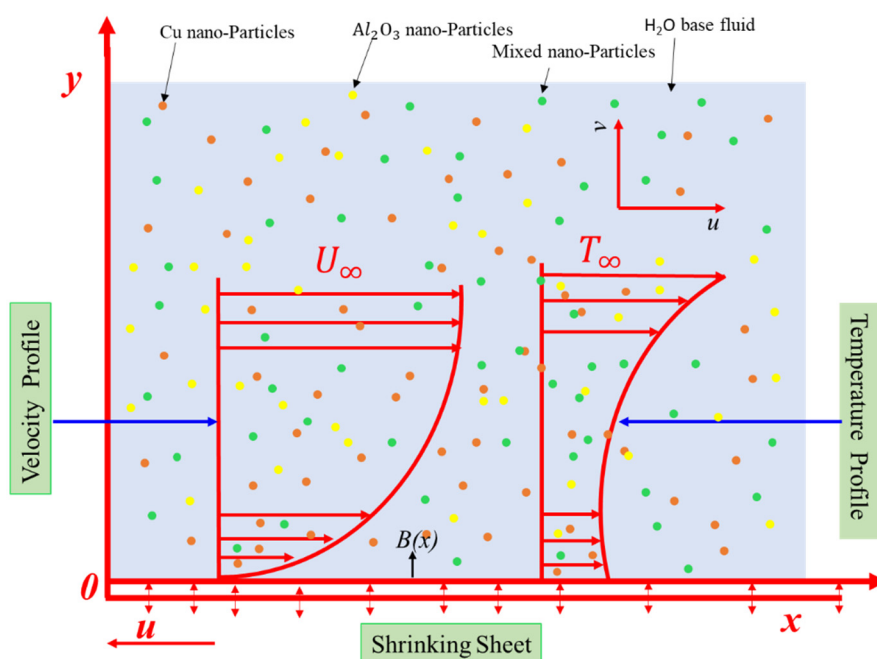


Figure 1. Physical model and coordinate system.

In the current work, we use the thermophysical features of nanomaterials, base fluid, and thermophysical properties of hybrid nanofluid [51]. In these regards, Tables 1 and 2 are presented.

Table 1. Properties of thermophysical of hybrid nanofluid.

Names	Properties
Viscosity of Dynamic	$\mu_{hnf} = \frac{\mu_f}{(1-\phi_{Cu})^{2.5}(1-\phi_{Al_2O_3})^{2.5}}$
Density	$\rho_{hnf} = (1 - \phi_{Cu})[(1 - \phi_{Al_2O_3})\rho_f + \phi_{Al_2O_3}\rho_{Al_2O_3}] + \phi_{Cu}\rho_{Cu}$
Thermal conductivity	$k_{hnf} = \frac{k_{Cu} + 2k_{nf} - 2\phi_{Cu}(k_{nf} - k_{Cu})}{k_{Cu} + 2k_{nf} + \phi_{Cu}(k_{nf} - k_{Cu})} \times (k_{nf})$ where $k_{nf} = \frac{k_{Al_2O_3} + 2k_f - 2\phi_{Al_2O_3}(k_f - k_{Al_2O_3})}{k_{Al_2O_3} + 2k_f + \phi_{Al_2O_3}(k_f - k_{Al_2O_3})} \times (k_f)$
Heat capacity	$(\rho c_p)_{hnf} = (1 - \phi_{Cu})[(1 - \phi_{Al_2O_3})(\rho c_p)_f + \phi_{Al_2O_3}(\rho c_p)_{Al_2O_3}] + \phi_{Cu}(\rho c_p)_{Cu}$
Electrical conductivity	$\sigma_{hnf} = \frac{\sigma_{Cu} + 2\sigma_{nf} - 2\phi_{Cu}(\sigma_{nf} - \sigma_{Cu})}{\sigma_{Cu} + 2\sigma_{nf} + \phi_{Cu}(\sigma_{nf} - \sigma_{Cu})} \times (\sigma_{nf})$ where $\sigma_{nf} = \frac{\sigma_{Al_2O_3} + 2\sigma_f - 2\phi_{Al_2O_3}(\sigma_f - \sigma_{Al_2O_3})}{\sigma_{Al_2O_3} + 2\sigma_f + \phi_{Al_2O_3}(\sigma_f - \sigma_{Al_2O_3})} \times (\sigma_f)$

Table 2. The thermal properties of nanoparticles and water.

Fluids	ρ (kg/m ³)	c_p (J/kg K)	k (W/m K)
Alumina (Al ₂ O ₃)	3970	765	40
Copper (Cu)	8933	385	400
Water (H ₂ O)	997.1	4179	0.613

To reduce the system into ODEs, we have the following variables of similarity transformation

$$\psi = \sqrt{2\vartheta_f l U_w} e^{\frac{x}{2l}} f(\eta); \theta(\eta) = \frac{T - T_\infty}{T_w - T_\infty}; \eta = y \sqrt{\frac{U_w}{2\vartheta_f l}} e^{\frac{x}{2l}} \tag{5}$$

where stream function is ψ and velocities are explained as $u = \frac{\partial\psi}{\partial y}$ and $v = -\frac{\partial\psi}{\partial x}$. By substituting Equation (5) in the Equations (2) and (3), which implies that

$$f''' + \xi_1 \{f'' f - 2(f')^2\} - \left[\gamma + \frac{\sigma_{hnf}}{\sigma_f} \xi_2 M \right] f' = 0 \tag{6}$$

$$\frac{k_{hnf}/k_f}{Pr \xi_3} \theta'' + \theta' f - \theta f' + \frac{Ec}{\xi_2 \xi_3} (f'')^2 = 0 \tag{7}$$

$$\begin{cases} \xi_1 = \xi_2 \left\{ (1 - \phi_{Cu}) \left[1 - \phi_{Al_2O_3} + \phi_{Al_2O_3} \left(\frac{\rho_{Al_2O_3}}{\rho_f} \right) \right] + \phi_{Cu} \left(\frac{\rho_{Cu}}{\rho_f} \right) \right\} \\ \xi_2 = (1 - \phi_{Cu})^{2.5} (1 - \phi_{Al_2O_3})^{2.5} \\ \xi_3 = \left\{ (1 - \phi_{Cu}) \left[1 - \phi_{Al_2O_3} + \phi_{Al_2O_3} \frac{(\rho c_p)_{Al_2O_3}}{(\rho c_p)_f} \right] + \phi_{Cu} \frac{(\rho c_p)_{Cu}}{(\rho c_p)_f} \right\} \end{cases} \tag{8}$$

Along with boundary conditions

$$\begin{cases} f(0) = S, f'(0) = -1, \theta(0) = 1 \\ f'(\eta) \rightarrow 0; \theta(\eta) \rightarrow 0 \text{ as } \eta \rightarrow \infty \end{cases} \tag{9}$$

where $M = \frac{2l\sigma_f(B_0)^2}{\rho_f U_w}$ is the magnetic number $\gamma = \frac{l\vartheta_f}{U_w K_0}$ is the permeability parameter, $Pr = \frac{\sigma_f}{\alpha_f}$ is Prandtl number, and $Ec = \frac{U_w^2}{(C_p)_f T_0}$ is Eckert number.

The significant physical factors are skin friction coefficient C_f and local Nusselt number Nu_x and explained as

$$C_f = \frac{\mu_{hnf}}{\rho_f u_w^2} \left(\frac{\partial u}{\partial y} \right) \Big|_{y=0}, Nu_x = -\frac{x k_{hnf}}{k_f (T_w - T_\infty)} \left(\frac{\partial T}{\partial y} \right) \Big|_{y=0} \tag{10}$$

By using Equation (5), these are obtained

$$\sqrt{Re} C_f = \frac{1}{\xi_2} f''(0); \sqrt{\frac{1}{Re}} Nu_x = -\frac{k_{hnf}}{k_f} \theta'(0) \tag{11}$$

3. Stability Analysis

To perform a stability analysis of the solution, the governing Equations (2) and (3) are needed to be reduced to unsteady flow problems. Thus, we get

$$\frac{\partial u}{\partial t} + u \frac{\partial u}{\partial x} + v \frac{\partial u}{\partial y} = \frac{\mu_{nf}}{\rho_{nf}} \frac{\partial^2 u}{\partial y^2} - \frac{\mu_{hnf}}{\rho_{hnf} K} u - \frac{\sigma_{hnf}}{\rho_{hnf}} B^2 u \tag{12}$$

$$\frac{\partial T}{\partial t} + u \frac{\partial T}{\partial x} + v \frac{\partial T}{\partial y} = \alpha_{nf} \frac{\partial^2 T}{\partial y^2} + \frac{\mu_{hmf}}{(\rho c_p)_{hmf}} \left(\frac{\partial u}{\partial y} \right)^2 \quad (13)$$

By introducing a time dependent variable τ , we have the following new non-dimensionless similarity transformation variables as mentioned in the paper of Lund et al. [54]:

$$\psi = \sqrt{2\vartheta l U_w} e^{\frac{x}{2l}} f(\eta, \tau); \quad \eta = y \sqrt{\frac{U_w}{2\vartheta l}} e^{\frac{x}{2l}}; \quad \tau = \frac{U_w}{2l} e^{\frac{x}{l}} t; \quad \theta(\eta, \tau) = \frac{(T - T_\infty)}{(T_w - T_\infty)} \quad (14)$$

By substituting Equation (14) into Equations (12) and (13), we have

$$\frac{\partial^3 f(\eta, \tau)}{\partial \eta^3} + \xi_1 \left\{ \frac{\partial^2 f(\eta, \tau)}{\partial \eta^2} f(\eta, \tau) - 2 \left(\frac{\partial f(\eta, \tau)}{\partial \eta} \right)^2 - \frac{\partial^2 f(\eta, \tau)}{\partial \tau \partial \eta} \right\} - \left[\gamma + \frac{\sigma_{hmf}}{\sigma_f} \xi_2 M \right] \frac{\partial f(\eta, \tau)}{\partial \eta} = 0 \quad (15)$$

$$\frac{k_{hmf}/k_f}{Pr \xi_3} \frac{\partial^2 \theta(\eta, \tau)}{\partial \eta^2} + f(\eta, \tau) \frac{\partial \theta(\eta, \tau)}{\partial \eta} - \frac{\partial f(\eta, \tau)}{\partial \eta} \theta(\eta, \tau) + \frac{Ec}{\xi_2 \xi_3} \left(\frac{\partial^2 f(\eta, \tau)}{\partial \eta^2} \right)^2 - \frac{\partial \theta(\eta, \tau)}{\partial \tau} = 0 \quad (16)$$

Along with boundary conditions

$$\begin{cases} f(0, \tau) = S, \frac{\partial f}{\partial \eta}(0, \tau) = -1, \theta(0, \tau) = 1 \\ f'(\eta, \tau) \rightarrow 0, \theta(\eta, \tau) \rightarrow 0 \text{ as } \eta \rightarrow \infty \end{cases} \quad (17)$$

To test the stability analysis of solutions of the steady-state flow, we have $f(\eta) = f_0(\eta)$ and $\theta(\eta) = \theta_0(\eta)$ which must satisfy the boundary value problems (BVPs) (6)–(9), we have

$$\theta(\eta, \tau) = \theta_0(\eta) + e^{-\varepsilon \tau} G(\eta, \tau); \quad f(\eta, \tau) = f_0(\eta) + e^{-\varepsilon \tau} F(\eta, \tau) \quad (18)$$

here, $G(\eta, \tau)$ and $F(\eta, \tau)$ and are the small concerned to $\theta_0(\eta)$. Additionally, $f_0(\eta)$ and ε is the unknown eigenvalue and the solutions of eigenvalues problems (16)–(18) provide an unlimited set of the eigenvalues $\varepsilon_1 < \varepsilon_2 < \varepsilon_3 \dots$. Substituting Equation (18) into Equations (15)–(17). The solutions $f(\eta) = f_0(\eta)$ and $\theta(\eta) = \theta_0(\eta)$ of steady state Equations (8) and (9) are found by setting $\tau = 0$. Thus, we have to solve the following linear eigenvalues problems.

$$F_0''' + \xi_1 \{ f_0 F_0'' + F_0 f_0'' - 4 f_0' F_0' + \varepsilon F_0' \} - \left[\gamma + \frac{\sigma_{hmf}}{\sigma_f} \xi_2 M \right] F_0' = 0 \quad (19)$$

$$\frac{k_{hmf}/k_f}{Pr \xi_3} G_0'' + f_0 G_0' + F_0 \theta_0' - f_0' G_0 - F_0' \theta_0 + \frac{2Ec}{\xi_2 \xi_3} f_0' F_0'' + \varepsilon G_0 = 0 \quad (20)$$

Along with reduced boundary conditions

$$\begin{cases} F_0(0) = 0, F_0'(0) = 0, G_0(0) = 0 \\ F_0'(\eta) \rightarrow 0, G_0(\eta) \rightarrow 0 \text{ as } \eta \rightarrow \infty \end{cases} \quad (21)$$

Harris et al. [55] proposed that in order to obtain the ε_1 , one boundary condition should be relaxed. Therefore, in this problem $F_0'(\eta) \rightarrow 0$ as $\eta \rightarrow \infty$ is relaxed to a new initial condition such that $F_0''(0) = 1$.

4. Results and Discussion

In this section, we discuss the results of the considered flow problem. Before going on to discuss the results, our numerical method is needed to validate and check the accuracy of the used method. For the validation, the values of $\sqrt{Re} C_f$ has been compared with the outcomes of Waini et al. [51] in Figure 2 graphically. The results show the same features as those noticed in the published paper (refer to Figure 2 of Waini et al. [51]). The results found excellent agreements as the critical values of

S_c of the current study are the same up to three decimal points those gotten by the Waini et al. [51]. Therefore, the three-stage Lobatto IIIa formula can be used confidently in this problem. The detailed description of this method can be seen in Lund et al.'s paper [54] and Rehman et al.'s paper [56]. Moreover, the present values of $f''(0)$ and $-\theta'(0)$ are correspondingly given in Tables 3 and 4.

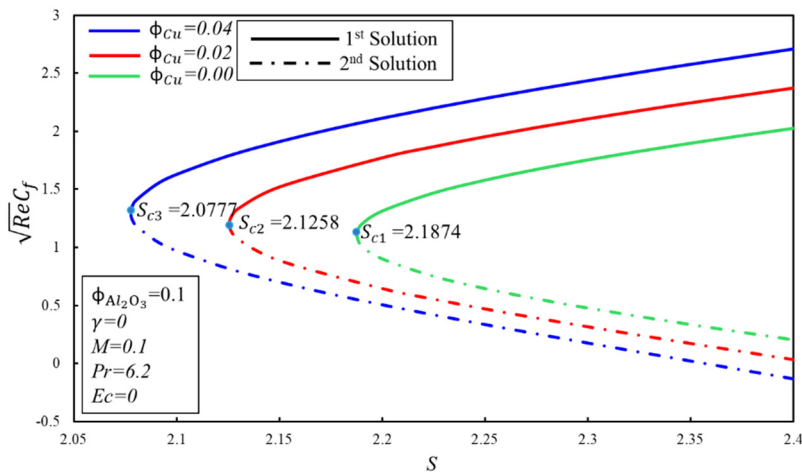


Figure 2. Variation of $\sqrt{Re}C_f$ for the comparison with Waini et al. [51].

Table 3. Outcomes of $f''(0)$ surface where $Pr = 6.2$, $\phi_{Al_2O_3} = 0.1$, and $Ec = 0.3$.

ϕ_{Cu}	M	γ	S	$f''(0)$			
				First Solution	Second Solution		
0.01	0	0	3	2.4863	-1.1077		
0.05				2.8189	-1.6261		
0.1				3.0749	-2.0807		
				0.1	3.1146	-2.2302	
				0.3	3.1908	-2.5230	
				0.5	3.2633	-2.8077	
				0.1	3.2967	-2.9403	
					0.3	3.3614	-3.1999
					0.5	3.4236	-3.4519
						2.75	3.0944
			2.5	2.7590	-1.6382		
			2.25	2.4142	-1.0062		

Table 4. The results of $-\theta'(0)$ where $\gamma = 0$, $\phi_{Al_2O_3} = 0.1$, and $S = 3$.

ϕ_{Cu}	Pr	M	Ec	$-\theta'(0)$			
				First Solution	Second Solution		
0.01	6.2	0	0	12.7302	12.5387		
0.05				11.2238	10.9591		
0.1				9.6302	9.2758		
				5	7.6893	7.2426	
				3	4.4876	3.7171	
				2	2.9193	1.8444	
				0.1	9.6319	9.2613	
					0.3	9.6354	9.2315
					0.5	9.6386	9.2000
						0.1	8.5867
			0.3	6.4827	0.6929		
			0.5	4.3787	7.2883		

From Figures 3–8, it is noticed that the similarity solutions of a system of reduced ODEs have a non-uniqueness of solutions in certain ranges of M and S . It should be noted that there does not exist a similarity solution when $S_c > S$ and $M_c > M$. Further, S_c and M_c are respective critical values of S and M where solutions exist. Variation of $f''(0)$ for numerous permeability parameter γ values is displayed in Figure 3 where $\phi_{Al_2O_3} = 0.1$, $\phi_{Cu} = 0.04$, $M = 0.5$, $Pr = 6.2$, and $Ec = 0.3$ are kept constant. It is noticed that for confident ranges of the S there are two solutions. Further, $S_{c1} = 1.7758$, $S_{c2} = 1.6169$, and $S_{c3} = 1.4463$ are the critical values for the respective $\gamma = 0$, $\gamma = 0.2$, and $\gamma = 0.4$. It is also examined that an increase in γ creates the enhancement in the coefficient of skin friction for the stable solution, while the reverse tendency is noted for the unstable solution. Physically, the reduction in skin friction is caused by the suction force that facilitates the separation of the boundary layer in the second solution. This nature of flow happens because of the pressure gradient and the antagonistic roles of transpiration on the fluid flow.

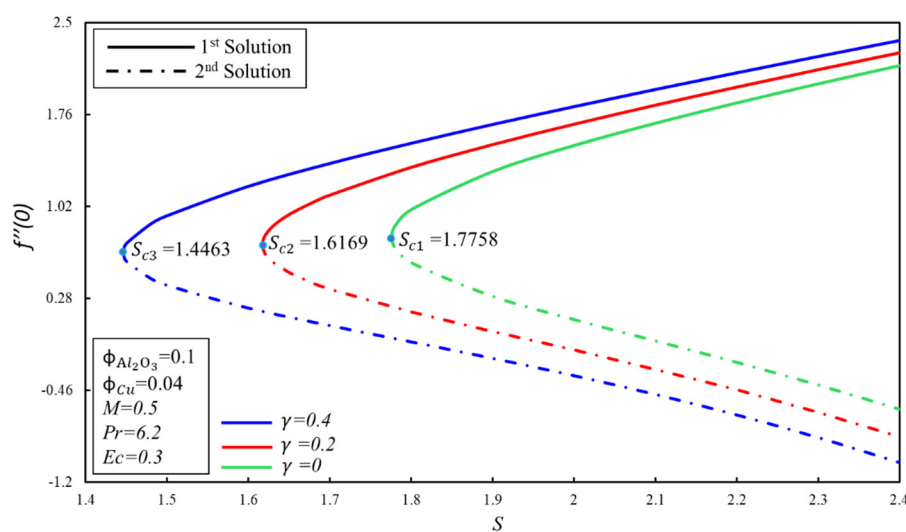


Figure 3. Variation of $f''(0)$ with γ for various values of S .

Figures 4 and 5 demonstrate the effect of ϕ_{Cu} on $f''(0)$ and $-\theta'(0)$ for several values of M by keeping $\phi_{Al_2O_3} = \gamma = 0.1$, $S = 1.75$, $Pr = 6.2$, and $Ec = 0.3$ constant. It is found that the higher ϕ_{Cu} values postpone separation of the layer since the ϕ_{Cu} 's critical values shift to the left. The coefficient of skin friction increases when Hartmann number M and copper volume fraction ϕ_{Cu} are increased in the first solution, but the contradictory trend of $f''(0)$ is found in the second solution. Furthermore, heat transfer enhances in a stable solution for the intensity of the magnetic effect, while it reduces in the second solution. Physically, the explanation of these natures can be explained as “the Lorentz force suppressed the vorticity produced by the shrinking of the sheet inside the boundary layer” [57]. The critical values of $\phi_{Cu} = 0.001$, $\phi_{Cu} = 0.01$, and $\phi_{Cu} = 0.1$ are $M_{c1} = 0.4885$, $M_{c2} = 0.4768$, and $M_{c3} = 0.3718$, respectively.

Figures 6 and 7 were drawn to demonstrate the effect of ϕ_{Cu} and S on $f''(0)$ and $-\theta'(0)$, respectively. Usually, flow over the shrinking surface generates the vorticity, therefore solutions do not occur subsequently vorticity has not been restricted inside the boundary layer. It is noticed from figures, so enough suction efficiency is required to sustain the fluid flow on a shrinking surface. These findings and behavior of fluid flow are supported by the statements of the Miklavčič and Wang [58] and Fang [59]. For high S values in the first solution, the rate of heat transfer and skin friction coefficient increase monotonically, while skin friction in the second solution decreases, but the rate of heat transfer upsurges initially for some instances and then starts to decrease. Further, $S_{c1} = 1.7401$, $S_{c2} = 1.6973$, and $S_{c3} = 1.6747$ are the critical values for the respective $\phi_{Cu} = 0.0$, $\phi_{Cu} = 0.02$, and $\phi_{Cu} = 0.04$.

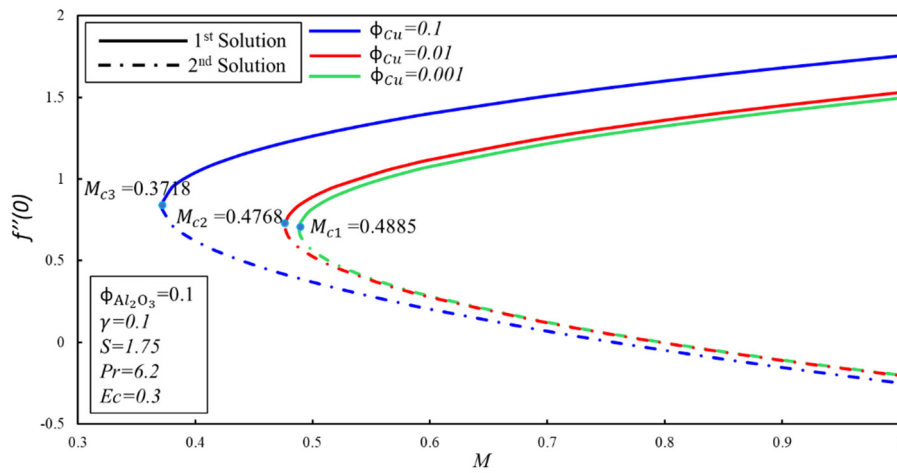


Figure 4. Variation of $f''(0)$ with ϕ_{Cu} for various values of M .

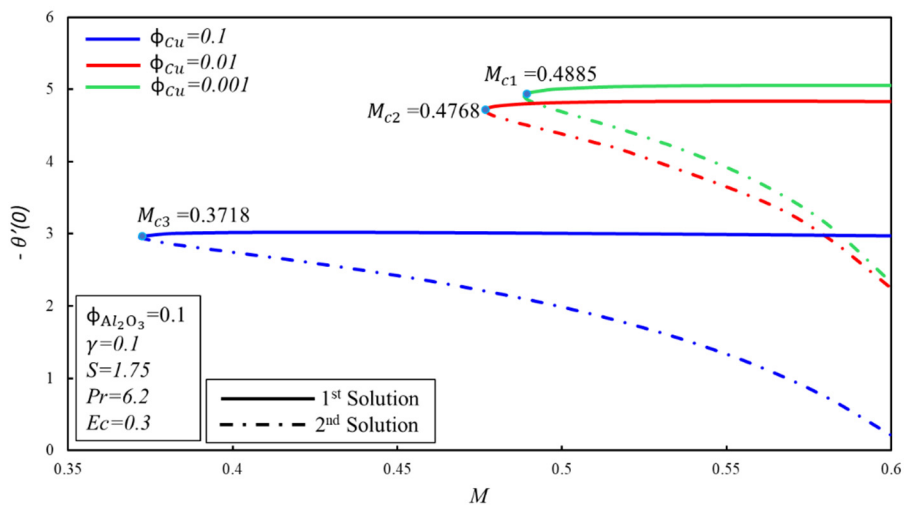


Figure 5. Variation of $-\theta'(0)$ with ϕ_{Cu} for various values of M .

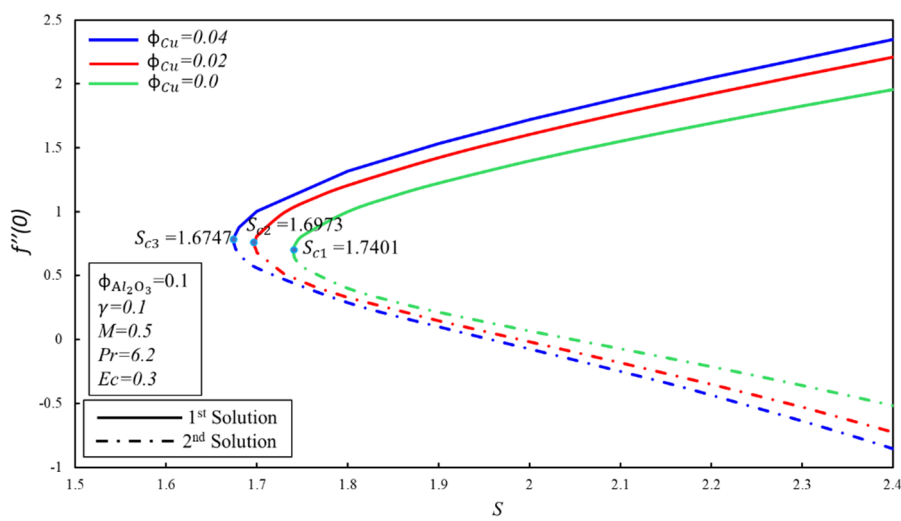


Figure 6. Variation of $f''(0)$ with ϕ_{Cu} for various values of S .

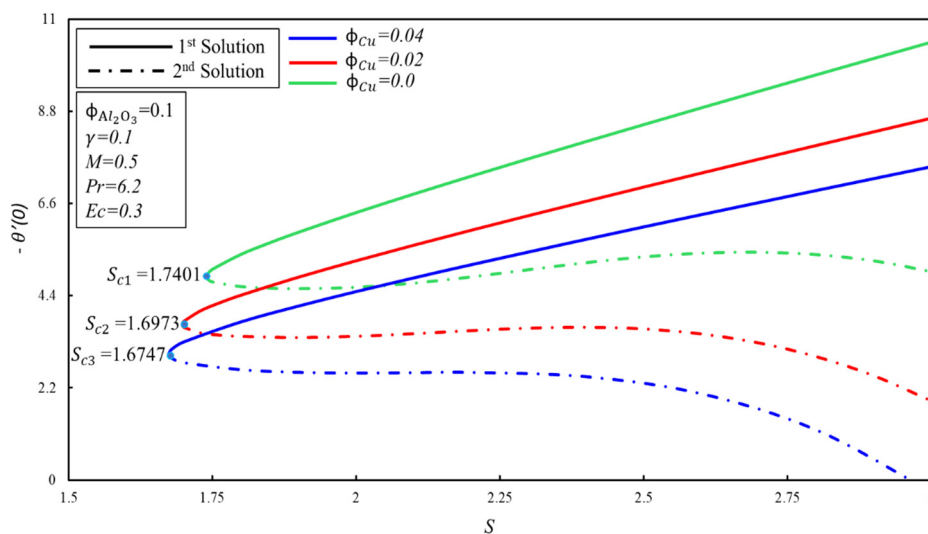


Figure 7. Variation of $-\theta'(0)$ with ϕ_{Cu} for various values of S .

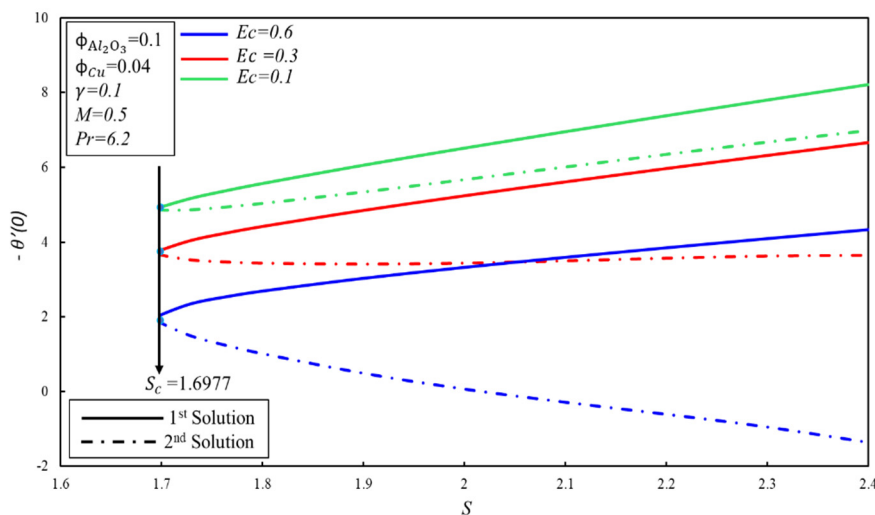


Figure 8. Variation of $-\theta'(0)$ with Ec for various values of S .

The effect of Eckert number on $-\theta'(0)$ is shown in Figure 8 where $\phi_{Al_2O_3} = \gamma = 0.1$, $\phi_{Cu} = 0.04$, $M = 0.5$, and $Pr = 6.2$ are kept as the constant. First solution demonstrates that the rate of heat transfer increases, while it reduces (enhances) for $Ec = 0.3, 0.6$ ($Ec = 0.1$) for the unstable solution. The effect of permeability γ on profiles of velocity $f'(\eta)$ and temperature $\theta(\eta)$ was drawn in Figures 9 and 10. It should be noted that for $f'(\eta)$ and $\theta(\eta)$ profiles, dual solutions exist and these profiles fulfill infinite boundary conditions asymptotically. It is examined that the increment of γ contributes to the rise of $f'(\eta)$ and $\theta(\eta)$ in the second solution, while no large variation is perceived in the first solution. It is examined that the velocity of the hybrid nanofluid reduces in the first solution when the porosity enhances. Physically, it shows that resistance exists due to the direct effect on the viscosity of the fluid. The effect of Ec on the profile of temperature $\theta(\eta)$ is revealed in Figure 11. We also found that the fluid temperature rises with the rising Ec values for both branches. Physically, the increase in Eckert number can be clarified in order to minimize enthalpy influence.

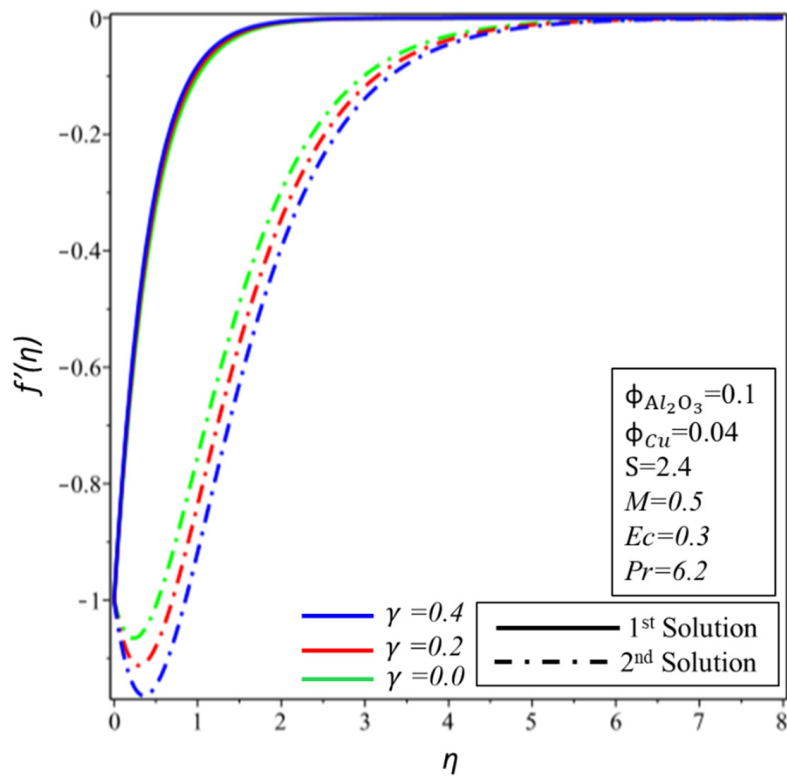


Figure 9. Variation of $f'(\eta)$ with η for various values of γ .

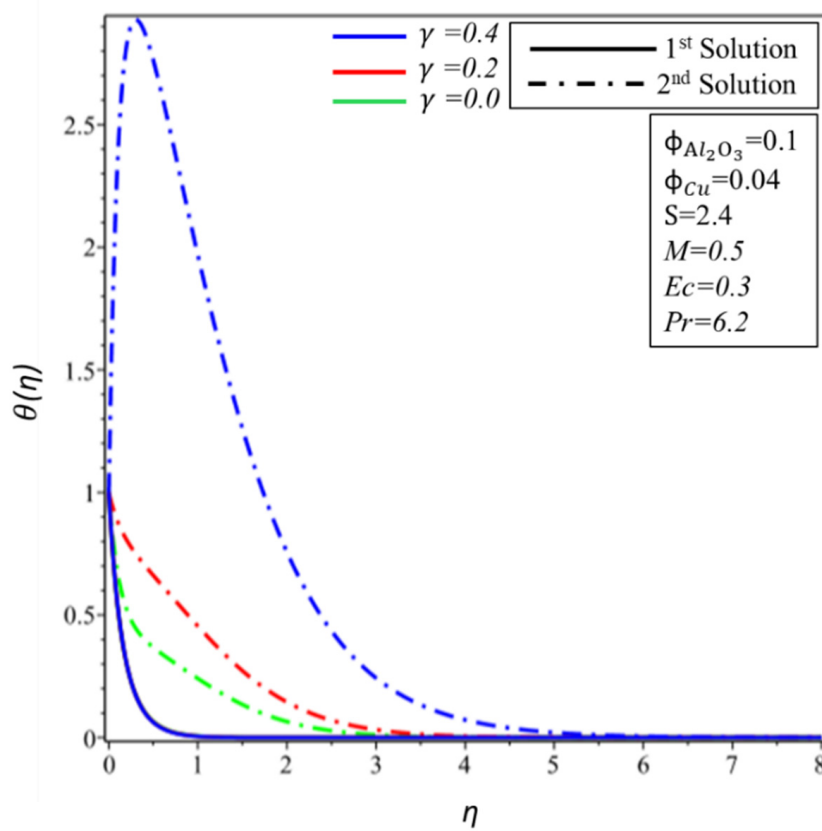


Figure 10. Variation of $\theta(\eta)$ with η for various values of γ .

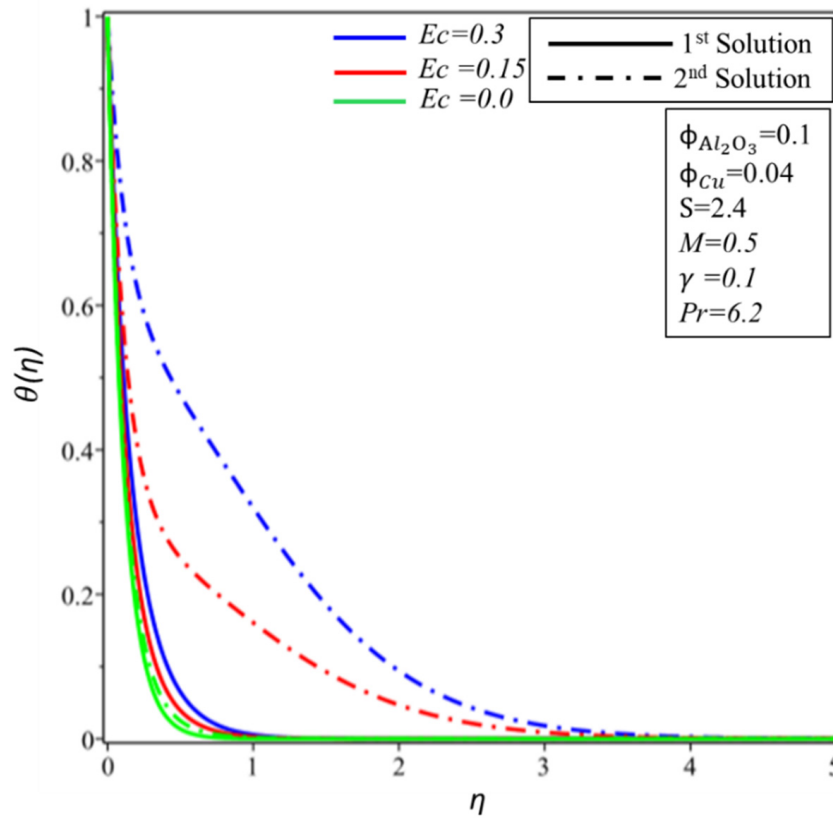


Figure 11. Variation of $\theta(\eta)$ with η for various values of Ec .

The graph of the values of the smallest eigenvalue ε_1 against suction S is depicted in Figure 12. According to Hamid et al. [60], positive (negative) values of γ show initial growth of decay (disturbance), and the solution of flow can be stable (unstable). From Figure 12, the first solution is clearly stable and the second one is unstable. Moreover, the graph of the smallest eigenvalue shows symmetrical behavior.

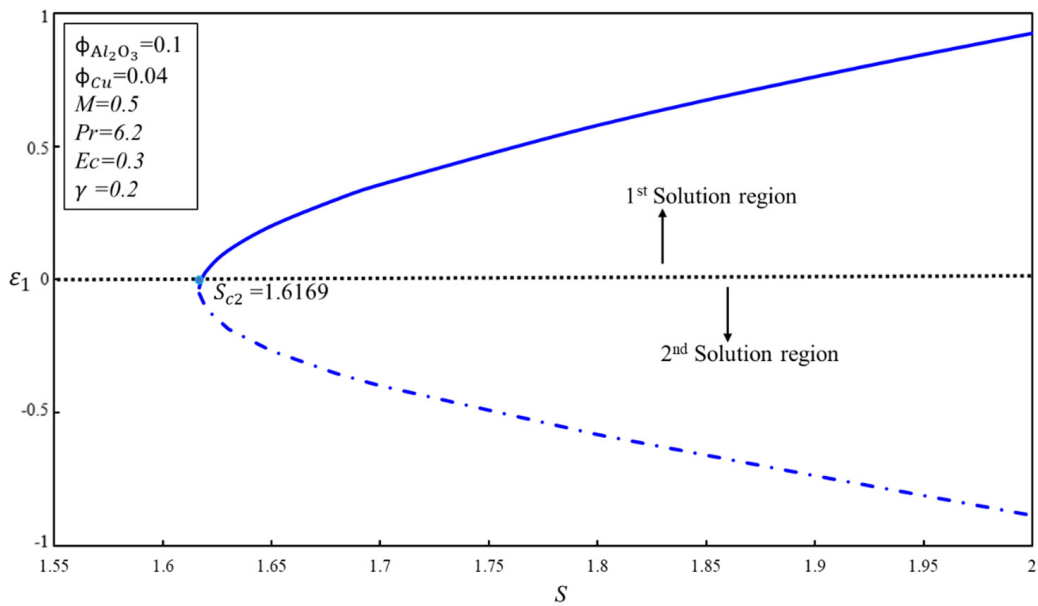


Figure 12. Smallest eigenvalues ε_1 for various values of S .

5. Conclusions

The effect of MHD flow of hybrid nanofluid on the exponentially permeable shrinking surface with the porous medium in the presence of viscous dissipation is examined. The effect of numerous emerging physical parameters on the heat transfer of hybrid nanofluid flow has been examined from the figures, and can be summarized as follows:

1. The present results show good agreements with the previously published results.
2. Dual solutions exist when $S_c \leq S$ and $M_c \leq M$, while no solution exists $S_c > S$ and $M_c > M$.
3. Shear stress rises in the first solution then declines in the second solution for the rising values of ϕ_{Cu} , M , S , and γ .
4. For the first solution, the heat transfer rate rises as S and M parameters are enhanced, while this is lower when ϕ_{Cu} is up.
5. Enhancement in the volume fraction of the nanoparticles pushes forward the boundary layer separation. Therefore, ranges of solutions increase.
6. Compared with nanofluid and viscous fluid, hybrid nanofluid seems to be more efficient in cooling processes.
7. The first is stable, and the second is unstable.
8. The Eckert number and temperature profiles are directly proportional.
9. The highest value of Eckert number does not affect the boundary layer separation against suction.
10. This model does not function outside the critical points, so there is no solution.

Author Contributions: L.A.L. derived the equations and generated the results and wrote the paper. Z.O. formulated the model and proofread the manuscript. S.D. helped to construct the model and derived the equations of stability. I.K. checked the whole manuscript and generated the stability values. D.B., and K.S.N. paid the APC of the journal, helped to revise the manuscript and read the revised version. All authors have read and agreed to the published version of the manuscript.

Funding: This research received no external funding.

Acknowledgments: The authors express their gratitude to the anonymous reviewers for their insightful comments and suggestions. The first author (L.A.L.) would like to thank his colleagues Waqar Hafeez, Adnan Asghar and Kashif Hussain for their moral support during the conduct of this research. Lastly, L.A.L. would like to appreciate and acknowledge the services provided by Makhdoom Ansari and Melati Puteh during the conduct of this research.

Conflicts of Interest: The authors declare no conflict of interest.

References

1. Choi, S.U.; Eastman, J.A. *Enhancing Thermal Conductivity of Fluids with Nanoparticles*; No. ANL/MSD/CP-84938; CONF-951135-29; Argonne National Lab.: Argonne, IL, USA, 1995.
2. Ahmad, M.; Muhammad, T.; Ahmad, I.; Aly, S. Time-dependent 3D flow of viscoelastic nanofluid over an unsteady stretching surface. *Phys. A Stat. Mech. Appl.* **2020**, *124*, 004. [[CrossRef](#)]
3. Ghazvini, M.; Maddah, H.; Peymanfar, R.; Ahmadi, M.H.; Kumar, R. Experimental evaluation and artificial neural network modeling of thermal conductivity of water based nanofluid containing magnetic copper nanoparticles. *Phys. A Stat. Mech. Appl.* **2020**, *124*, 127. [[CrossRef](#)]
4. Tassaddiq, A.; Khan, I.; Nisar, K.S. Heat transfer analysis in sodium alginate based nanofluid using MoS₂ nanoparticles: Atangana–Baleanu fractional model. *Chaos Solitons Fractals* **2020**, *130*, 109445. [[CrossRef](#)]
5. Nadeem, S.; Abbas, N.; Elmasry, Y.; Malik, M.Y. Numerical analysis of water based CNTs flow of micropolar fluid through rotating frame. *Comput. Methods Programs Biomed.* **2020**, *186*, 105194. [[CrossRef](#)]
6. Mitra, D.; Howli, P.; Das, B.K.; Das, N.S.; Chattopadhyay, P.; Chattopadhyay, K.K. Size and phase dependent thermal conductivity of TiO₂-water nanofluid with theoretical insight. *J. Mol. Liq.* **2020**, *302*, 112499. [[CrossRef](#)]
7. Sahoo, R.R.; Kumar, V. Development of a new correlation to determine the viscosity of ternary hybrid nanofluid. *Int. Commun. Heat Mass Transf.* **2020**, *111*, 104451. [[CrossRef](#)]

8. Shafiq, A.; Khan, I.; Rasool, G.; Sherif, E.S.M.; Sheikh, A.H. Influence of Single-and Multi-Wall Carbon Nanotubes on Magnetohydrodynamic Stagnation Point Nanofluid Flow over Variable Thicker Surface with Concave and Convex Effects. *Mathematics* **2020**, *8*, 104. [[CrossRef](#)]
9. Giresha, B.J.; Umshaiah, M.; Prasannakumara, B.C.; Shashikumar, N.S.; Archana, M. Impact of nonlinear thermal radiation on magnetohydrodynamic three dimensional boundary layer flow of Jeffrey nanofluid over a nonlinearly permeable stretching sheet. *Phys. A Stat. Mech. Appl.* **2020**, 124051. [[CrossRef](#)]
10. Lund, L.A.; Omar, Z.; Khan, U.; Khan, I.; Baleanu, D.; Nisar, K.S. Stability Analysis and Dual Solutions of Micropolar Nanofluid over the Inclined Stretching/Shrinking Surface with Convective Boundary Condition. *Symmetry* **2020**, *12*, 74. [[CrossRef](#)]
11. Ghasemi, H.; Aghabarari, B.; Alizadeh, M.; Khanlarkhani, A.; Abu-Zahra, N. High efficiency decolorization of wastewater by Fenton catalyst: Magnetic iron-copper hybrid oxides. *J. Water Process Eng.* **2020**, *37*, 101540. [[CrossRef](#)]
12. Rasool, G.; Shafiq, A.; Baleanu, D. Consequences of Soret–Dufour Effects, Thermal Radiation, and Binary Chemical Reaction on Darcy Forchheimer Flow of Nanofluids. *Symmetry* **2020**, *12*, 1421. [[CrossRef](#)]
13. Mozaffari, S. Rheology of Bitumen at the Onset of Asphaltene Aggregation and Its Effects on the Stability of Water-In-Oil Emulsion. Master’s Thesis, University of Alberta, Alberta, AB, Canada, 2015. [[CrossRef](#)]
14. Darjani, S.; Koplik, J.; Banerjee, S.; Pauchard, V. Liquid-hexatic-solid phase transition of a hard-core lattice gas with third neighbor exclusion. *J. Chem. Phys.* **2019**, *151*, 104702. [[CrossRef](#)] [[PubMed](#)]
15. Shafiq, A.; Rasool, G.; Khalique, C.M. Significance of thermal slip and convective boundary conditions in three dimensional rotating Darcy-Forchheimer nanofluid flow. *Symmetry* **2020**, *12*, 741. [[CrossRef](#)]
16. Mozaffari, S.; Li, W.; Dixit, M.; Seifert, S.; Lee, B.; Kovarik, L.; Mpourmpakis, G.; Karim, A.M. The role of nanoparticle size and ligand coverage in size focusing of colloidal metal nanoparticles. *Nanoscale Adv.* **2019**, *1*, 4052–4066. [[CrossRef](#)]
17. Darjani, S.; Koplik, J.; Pauchard, V. Extracting the equation of state of lattice gases from random sequential adsorption simulations by means of the Gibbs adsorption isotherm. *Phys. Rev. E* **2017**, *96*, 052803. [[CrossRef](#)] [[PubMed](#)]
18. Shafiq, A.; Rasool, G.; Khalique, C.M.; Aslam, S. Second Grade Bioconvective Nanofluid Flow with Buoyancy Effect and Chemical Reaction. *Symmetry* **2020**, *12*, 621. [[CrossRef](#)]
19. Esfe, M.H.; Alirezaie, A.; Rejvani, M. An applicable study on the thermal conductivity of SWCNT-MgO hybrid nanofluid and price-performance analysis for energy management. *Appl. Therm. Eng.* **2017**, *111*, 1202–1210. [[CrossRef](#)]
20. Sundar, L.S.; Sharma, K.V.; Singh, M.K.; Sousa, A.C.M. Hybrid nanofluids preparation, thermal properties, heat transfer and friction factor—a review. *Renew. Sustain. Energy Rev.* **2017**, *68*, 185–198. [[CrossRef](#)]
21. Lund, L.A.; Omar, Z.; Khan, I.; Seikh, A.H.; Sherif, E.S.M.; Nisar, K.S. Stability analysis and multiple solution of Cu–Al₂O₃/H₂O nanofluid contains hybrid nanomaterials over a shrinking surface in the presence of viscous dissipation. *J. Mater. Res. Technol.* **2020**, *9*, 421–432. [[CrossRef](#)]
22. Devi, S.A.; Devi, S.S.U. Numerical investigation of hydromagnetic hybrid Cu–Al₂O₃/water nanofluid flow over a permeable stretching sheet with suction. *Int. J. Nonlinear Sci. Numer. Simul.* **2016**, *17*, 249–257. [[CrossRef](#)]
23. Suresh, S.; Venkataraj, K.P.; Selvakumar, P.; Chandrasekar, M. Synthesis of Al₂O₃–Cu/water hybrid nanofluids using two step method and its thermo physical properties. *Colloids Surf. A Physicochem. Eng. Asp.* **2011**, *388*, 41–48. [[CrossRef](#)]
24. Hayat, T.; Nadeem, S. Heat transfer enhancement with Ag–CuO/water hybrid nanofluid. *Results Phys.* **2017**, *7*, 2317–2324. [[CrossRef](#)]
25. Jamshed, W.; Aziz, A. Cattaneo–Christov based study of TiO₂–CuO/EG Casson hybrid nanofluid flow over a stretching surface with entropy generation. *Appl. Nanosci.* **2018**, *8*, 685–698. [[CrossRef](#)]
26. Rostami, M.N.; Dinarvand, S.; Pop, I. Dual solutions for mixed convective stagnation-point flow of an aqueous silica–alumina hybrid nanofluid. *Chin. J. Phys.* **2018**, *56*, 2465–2478. [[CrossRef](#)]
27. Aly, E.H.; Pop, I. MHD flow and heat transfer over a permeable stretching/shrinking sheet in a hybrid nanofluid with a convective boundary condition. *Int. J. Numer. Methods Heat Fluid Flow* **2019**. [[CrossRef](#)]
28. Khan, A.S.; Khan, M.I.; Hayat, T.; Faisal Javed, M.; Alsaedi, A. Mixed convective non-linear radiative flow with TiO₂-Cu-water hybrid nanomaterials and induced magnetic field. *Int. J. Numer. Methods Heat Fluid Flow* **2019**. [[CrossRef](#)]

29. Olatundun, A.T.; Makinde, O.D. Analysis of Blasius flow of hybrid nanofluids over a convectively heated surface. In *Defect and Diffusion Forum*; Trans Tech Publications: Stafa-Zurich, Switzerland, 2017; Volume 377, pp. 29–41.
30. Abbas, N.; Nadeem, S.; Malik, M.Y. Theoretical study of micropolar hybrid nanofluid over Riga channel with slip conditions. *Phys. A Stat. Mech. Appl.* **2020**, 124083. [[CrossRef](#)]
31. Maskeen, M.M.; Zeeshan, A.; Mehmood, O.U.; Hassan, M. Heat transfer enhancement in hydromagnetic alumina–copper/water hybrid nanofluid flow over a stretching cylinder. *J. Therm. Anal. Calorim.* **2019**, *138*, 1127–1136. [[CrossRef](#)]
32. Chamkha, A.J.; Dogonchi, A.S.; Ganji, D.D. Magneto-hydrodynamic flow and heat transfer of a hybrid nanofluid in a rotating system among two surfaces in the presence of thermal radiation and Joule heating. *AIP Adv.* **2019**, *9*, 025103. [[CrossRef](#)]
33. Khan, M.I.; Khan, S.A.; Hayat, T.; Waqas, M.; Alsaedi, A. Modeling and numerical simulation for flow of hybrid nanofluid ($\text{SiO}_2/\text{C}_3\text{H}_8\text{O}_2$) and ($\text{MoS}_2/\text{C}_3\text{H}_8\text{O}_2$) with entropy optimization and variable viscosity. *Int. J. Numer. Methods Heat Fluid Flow* **2019**. [[CrossRef](#)]
34. Sharma, A.K.; Singh, R.K.; Dixit, A.R.; Tiwari, A.K.; Singh, M. An Investigation on Tool Flank Wear Using Alumina/ MoS_2 Hybrid Nanofluid in Turning Operation. In *Advances in Manufacturing Engineering and Materials*; Springer: Cham, Switzerland, 2019; pp. 213–219.
35. Al-Mdallal, Q.M.; Indumathi, N.; Ganga, B.; Hakeem, A.A. Marangoni radiative effects of hybrid-nanofluids flow past a permeable surface with inclined magnetic field. *Case Stud. Therm. Eng.* **2020**, *17*, 100571. [[CrossRef](#)]
36. Ramesh, G.K. Three different hybrid nanometrial performances on rotating disk: A non-Darcy model. *Appl. Nanosci.* **2019**, *9*, 179–187. [[CrossRef](#)]
37. Lund, L.A.; Omar, Z.; Khan, I. Mathematical analysis of magnetohydrodynamic (MHD) flow of micropolar nanofluid under buoyancy effects past a vertical shrinking surface: Dual solutions. *Heliyon* **2019**, *5*, e02432. [[CrossRef](#)] [[PubMed](#)]
38. Ghadikolaei, S.S.; Gholinia, M.; Hoseini, M.E.; Ganji, D.D. Natural convection MHD flow due to MoS_2 –Ag nanoparticles suspended in $\text{C}_2\text{H}_6\text{O}_2/\text{H}_2\text{O}$ hybrid base fluid with thermal radiation. *J. Taiwan Inst. Chem. Eng.* **2019**, *97*, 12–23. [[CrossRef](#)]
39. Magyari, E.; Keller, B. Heat and mass transfer in the boundary layers on an exponentially stretching continuous surface. *J. Phys. D Appl. Phys.* **1999**, *32*, 577. [[CrossRef](#)]
40. Mushtaq, A.; Farooq, M.A.; Sharif, R.; Razaq, M. The impact of variable fluid properties on hydromagnetic boundary layer and heat transfer flows over an exponentially stretching sheet. *J. Phys. Commun.* **2019**, *3*, 095005. [[CrossRef](#)]
41. Reddy, G.B.; Goud, B.S.; Shekar, M.R. Numerical Solution of MHD Mixed Convective Boundary Layer Flow of a Nanofluid through a Porous Medium due to an Exponentially Stretching Sheet with Magnetic Field Effect. *Int. J. Appl. Eng. Res.* **2019**, *14*, 2074–2083.
42. Rahman, A.N.H.; Bachok, N.; Rosali, H. Numerical Solutions of MHD Stagnation-Point Flow over an Exponentially Stretching/Shrinking Sheet in a Nanofluid. In *Journal of Physics: Conference Series*; IOP Publishing: Bristol, UK, 2019; Volume 1366, p. 012012.
43. Farooq, U.; Lu, D.; Munir, S.; Ramzan, M.; Suleman, M.; Hussain, S. MHD flow of Maxwell fluid with nanomaterials due to an exponentially stretching surface. *Sci. Rep.* **2019**, *9*, 1–11. [[CrossRef](#)]
44. Dero, S.; Rohni, A.M.; Saaban, A. MHD micropolar nanofluid flow over an exponentially stretching/shrinking surface: Triple solutions. *J. Adv. Res. Fluid Mech. Therm. Sci.* **2019**, *56*, 165–174.
45. Lund, L.A.; Omar, Z.; Khan, I. Steady incompressible magnetohydrodynamics Casson boundary layer flow past a permeable vertical and exponentially shrinking sheet: A stability analysis. *Heat Transf. Asian Res.* **2019**, *48*, 3538–3556. [[CrossRef](#)]
46. Ali Lund, L.; Ching, D.L.C.; Omar, Z.; Khan, I.; Nisar, K.S. Triple local similarity solutions of Darcy-Forchheimer Magnetohydrodynamic (MHD) flow of micropolar nanofluid over an exponential shrinking surface: Stability analysis. *Coatings* **2019**, *9*, 527. [[CrossRef](#)]
47. Lund, L.A.; Omar, Z.; Khan, I.; Raza, J.; Sherif, E.S.M.; Seikh, A.H. Magnetohydrodynamic (MHD) Flow of Micropolar Fluid with Effects of Viscous Dissipation and Joule Heating Over an Exponential Shrinking Sheet: Triple Solutions and Stability Analysis. *Symmetry* **2020**, *12*, 142. [[CrossRef](#)]

48. Bachok, N.; Ishak, A.; Pop, I. Boundary layer stagnation-point flow and heat transfer over an exponentially stretching/shrinking sheet in a nanofluid. *Int. J. Heat Mass Transf.* **2012**, *55*, 8122–8128. [[CrossRef](#)]
49. Dzulkipli, N.; Bachok, N.; Yacob, N.; Md Arifin, N.; Rosali, H. Unsteady stagnation-point flow and heat transfer over a permeable exponential stretching/shrinking sheet in nanofluid with slip velocity effect: A stability analysis. *Appl. Sci.* **2018**, *8*, 2172. [[CrossRef](#)]
50. Anuar, N.S.; Bachok, N.; Arifin, N.M.; Rosali, H.; Pop, I. Stagnation-Point Flow and Heat Transfer over an Exponentially Stretching/Shrinking Sheet in Hybrid Nanofluid with Slip Velocity Effect: Stability Analysis. In *Journal of Physics: Conference Series*; IOP Publishing: Bristol, UK, 2019; Volume 1366, p. 012002.
51. Waini, I.; Ishak, A.; Pop, I. Hybrid nanofluid flow induced by an exponentially shrinking sheet. *Chin. J. Phys.* **2019**. [[CrossRef](#)]
52. Jain, S.; Choudhary, R. Effects of MHD on boundary layer flow in porous medium due to exponentially shrinking sheet with slip. *Procedia Eng.* **2015**, *127*, 1203–1210. [[CrossRef](#)]
53. Ali Lund, L.; Omar, Z.; Khan, I.; Raza, J.; Bakouri, M.; Tlili, I. Stability Analysis of Darcy-Forchheimer Flow of Casson Type Nanofluid Over an Exponential Sheet: Investigation of Critical Points. *Symmetry* **2019**, *11*, 412. [[CrossRef](#)]
54. Lund, L.A.; Omar, Z.; Khan, I. Quadruple solutions of mixed convection flow of magnetohydrodynamic nanofluid over exponentially vertical shrinking and stretching surfaces: Stability analysis. *Comput. Methods Programs Biomed.* **2019**, *182*, 105044. [[CrossRef](#)]
55. Harris, S.D.; Ingham, D.B.; Pop, I. Mixed convection boundary-layer flow near the stagnation point on a vertical surface in a porous medium: Brinkman model with slip. *Transp. Porous Media* **2009**, *77*, 267–285. [[CrossRef](#)]
56. Rahman, M.M.; Roşca, A.V.; Pop, I. Boundary layer flow of a nanofluid past a permeable exponentially shrinking/stretching surface with second order slip using Buongiorno's model. *Int. J. Heat Mass Transf.* **2014**, *77*, 1133–1143. [[CrossRef](#)]
57. Bhattacharyya, K.; Pop, I. MHD boundary layer flow due to an exponentially shrinking sheet. *Magnetohydrodynamics* **2011**, *47*, 337–344.
58. Miklavčič, M.; Wang, C. Viscous flow due to a shrinking sheet. *Q. Appl. Math.* **2006**, *64*, 283–290. [[CrossRef](#)]
59. Fang, T. Boundary layer flow over a shrinking sheet with power-law velocity. *Int. J. Heat Mass Transf.* **2008**, *51*, 5838–5843. [[CrossRef](#)]
60. Hamid, M.; Usman, M.; Khan, Z.H.; Ahmad, R.; Wang, W. Dual solutions and stability analysis of flow and heat transfer of Casson fluid over a stretching sheet. *Phys. Lett. A* **2019**, *383*, 2400–2408. [[CrossRef](#)]



© 2020 by the authors. Licensee MDPI, Basel, Switzerland. This article is an open access article distributed under the terms and conditions of the Creative Commons Attribution (CC BY) license (<http://creativecommons.org/licenses/by/4.0/>).